RSC Advances

PAPER

Cite this: *RSC Adv.*, 2022, **12**, 10366

Experimental study on pretreatment effects of [BMIM]HSO_4/ethanol on the thermal behavior of cellulose†

Huamei Yang, *[a] Ju Jiang,[a] Bingzhe Zhang,[a] Wenyuan Zhang,[a] Weining Xie[b] and Jing Li*[a]

Received 10th February 2022
Accepted 28th March 2022

DOI: 10.1039/d2ra00876a

rsc.li/rsc-advances

Ionic liquids (ILs) have been investigated to dissolve and/or pre-treat cellulose by combining with a low viscous co-solvent. Dissolution and pretreatment of cellulose by ILs are dynamic processes of dissolution and precipitation, which would caused the physical and chemical changes (such as crystallinity and thermal stability) of un-dissolved cellulose residues. Hence, this study focused on the thermal behavior of un-dissolved cellulose (PCEL) after pre-treatment using [BMIM]HSO_4/ethanol. Ethanol was used as a green and cheap co-solvent of 1-butyl-3-methylimidazolium hydrogen sulfate ([BMIM]HSO_4) to pre-treat cellulose under different conditions. The pretreatment effect on thermal behavior of PCEL was investigated by thermogravimetric analysis and the distributed activation energy model. [BMIM]HSO_4/ethanol pretreatment efficiently lowered the thermal stability of cellulose, and promoted the thermal decomposition at low temperature. The thermal behavior of PCEL can be adjusted by the [BMIM]HSO_4 mass concentration.

1. Introduction

Cellulose is the main component of lignocellulosic biomass, which is an extremely abundant feedstock naturally.[1,2] Cellulose is a polysaccharide consisting of linear chains of numerous β-D-glucans with chemical monomers $(C_6H_{10}O_5)_n$ linked by β-1,4-glycosidic bonds. There are numerous inter-molecular and intra-molecular hydrogen bonds in cellulose, leading to its difficulty to be converted into biofuels and value-added chemicals.[3–5] Hence to design reactors and optimize the process, appropriate pretreatment is necessary to improve the quality of cellulose, and decrease the energy requirement of thermal conversion.[3,6,7]

Ionic liquids (ILs) are salts with a wide liquidus range, good thermal stability, low vapor pressure, and are non-flammable. So ILs can provide a unique platform for chemical reactions and are seen as potential green replacements for volatile solvents.[8] Studies on the application of ILs in cellulose have been widely carried out, and many kinds of ILs have been found to be able to dissolve cellulose to serve as the reaction medium to functionalize cellulose.[8–12] Both the cation and anion of ILs influence the dissolution of cellulose. An efficient IL for dissolving cellulose should contain a small cation and a moderate donor to make H bonds with hydroxyl groups in the cellulose structure while anion is a good hydrogen bond acceptor in cellulose dissolution.[8,13] Published works reported that cellulose can be dissolved without any pretreatment in 1-butyl-3-methylimidazolium [BMIM] based ionic liquids.[10] Wang *et al.*,[8] Salama *et al.*[12] and Xu *et al.*[13] reviewed anions investigated are mainly OAc^-, $HCOO^-$, Cl^-, Br^-, $(MeO)_2PO_2^-$, $(C_6H_5)COO^-$ and HSO_4^-. Nis *et al.*[14] found that 1-butyl-3-methylimidazolium hydrogen sulfate ([BMIM]HSO_4) displayed the highest efficiency to convert cellulose into valuable chemicals which can be attributed to the acidic character of the ILs.

Besides H-bonding ability of ILs, solvent viscosity is also an important parameter due to the effects on mass transfer.[14] IL is always highly viscous, since there exists a strong interaction between cation and anion.[14,15] Hence, low viscous mixture systems have been developed with IL mixing with co-solvent such as dimethyl sulfoxide, *N*,*N*-dimethylforamide, *N*,*N*-dimethylacetamide, and *N*-methylpyrrolidinone.[11,13–20] These widely-used reagents are expensive and/or toxic. Ethanol is a green and cheap polar solvent, which can be produced from cellulose and biomass.[21] However, little is known about the dissolution performance of cellulose in the mixtures of ILs and ethanol. With the curiosity to know the effects of ILs and ethanol, this study developed a series mixture solvents of [BMIM]HSO_4 and ethanol ([BMIM]HSO_4/ethanol) to pre-treat cellulose under different conditions.

At the same time, it was noted that currently studies were mainly focused on the investigation of cellulose solubility,[8,11–13]

[a]School of Materials and Chemical Engineering, Xuzhou University of Technology, Xuzhou 221018, China. E-mail: yhmcumt@yeah.net; lijingxz111@163.com
[b]Advanced Analysis and Computation Center, China University of Mining and Technology, Xuzhou 221116, China

† Electronic supplementary information (ESI) available. See DOI: 10.1039/d2ra00876a

and the characterization of regenerated cellulose which was regenerated from ILs by addition of water, ethanol or acetone.[4,9] In fact, cellulose dissolution process was a dynamic process of dissolution and precipitation. The characters, such as crystalline and thermal stability of un-dissolved pre-treated cellulose (PCEL) are possibly changed after removed from ILs solvent.[22] However, there are very limited researches on the investigation of PCEL. Hence, we focused on PCEL pre-treated by [BMIM]HSO_4/ethanol, rather than the cellulose solution and regenerated cellulose. The main task in this study is to investigate the effects of [BMIM]HSO_4/ethanol on the thermal behavior of PCEL pre-treated under different conditions: pretreatment temperature at 80–200 °C, [BMIM]HSO_4 mass concentration in 0–60%, pretreatment time in 1–16 h, and solid–liquid mass ration in 1 : 1–1 : 20. [BMIM]HSO_4/ethanol was easily separated with PCEL by filtration, and reused to pre-treat cellulose without any further treatment.

2. Materials and methods

2.1 Materials

Microcrystalline cellulose (MCEL, lot #EK161201, purity ≥ 98%) was obtained from EKEAR (Shanghai, China). [BMIM]HSO_4 (as shown in Fig. 1) was obtained from Lanzhou Institute of Chemical Physics, Chinese Academy of Sciences. Ethanol (purity ≥ 99.8%) was obtained from Titan Scientific Company (Shanghai, China).

2.2 Cellulose pretreatment with the mixture of [BMIM]HSO_4 and ethanol

[BMIM]HSO_4 and ethanol were completely mixed in a conical flask with magnetic stirring (the rotating speed of 400 rpm). The mixture of [BMIM]HSO_4 and ethanol was named as [BMIM]HSO_4/ethanol. MCEL and [BMIM]HSO_4/ethanol were mixed in a PTFE-lined hydrothermal reactor, and heated in an electromagnetic stirring heater at an expected temperature with magnetic stirring (the rotating speed of 400 rpm). After [BMIM]HSO_4/ethanol pretreatment, cellulose sample and [BMIM]HSO_4/ethanol were separated by vacuum filtration. Filter liquor was the used [BMIM]HSO_4/ethanol, which can be reused to pre-treat MCEL without any treatment. After washed three times with ethanol, filter cake was dried in vacuum oven at 50 °C for 8 h. The dried filter cake was solid residues, PCEL. PCEL pre-treated by [BMIM]HSO_4/ethanol with different concentrations from 0% to 100% were named as PCEL0%–PCEL100%, respectively.

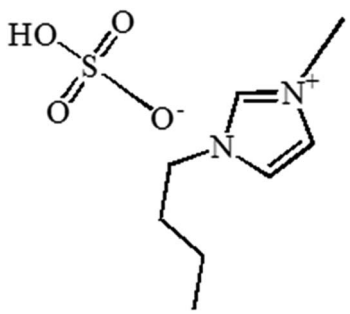

Fig. 1 Structure diagram of [BMIM]HSO_4.

2.3 Thermogravimetric analysis

A thermogravimetric analyzer (GAQ50, TA Instruments, U.S.) was used for the thermogravimetric analysis of MCEL and PCEL. The amount of material used in each experiment was about 10 mg. The carrier gas was nitrogen, and the flow rate was 60 mL min^{-1}. The heating procedure was set as: equilibrium at 120 °C, and then 20 °C min^{-1} heated to 650 °C. PCEL pre-treated by different [BMIM]HSO_4 concentration was also heated from 120 °C to 650 °C at different heating rates (20 °C min^{-1}, 40 °C min^{-1}, and 80 °C min^{-1}), which were used to analyze the effect of [BMIM]HSO_4 mass concentration on thermal behavior and to calculate the activation energy (E).

2.4 Kinetic analysis

Thermal decomposition kinetic parameters of MCEL and PCEL were determined by the distributed activation energy model (DAEM), which was widely used for biomass kinetics analysis. The model assumes that the thermal degradation of biomass is composed of an infinite number of first-order parallel reactions. E is estimated from the TG data is a continuous distribution function depending on the conversion rate (α) or temperature (T). The model is represented as eqn (1):

$$1 - V/V^* = \int_0^\infty \exp\left(-\frac{k}{\beta}\int_0^T e^{-E/RT}dT\right) f(E)dE \quad (1)$$

In which, V is the volatiles at the pyrolysis temperature of T, V^* is the effective content of volatiles, $f(E)$ is the distribution curve of activation energy. Other symbols of E, k, and β represent the activation energy, the frequency factor, the universal gas constant, respectively. In this study, α is defined as V/V^*, and could be calculated by eqn (2):

$$\alpha = \frac{m_0 - m_t}{m_0 - m_f} \quad (2)$$

In which, m_0 is the initial mass of samples, m_t is the actual mass of samples at the pyrolysis time of t, m_f is the final mass of samples. After a series of mathematical simplification and approximation, the DAEM model can be simplified to eqn (3):

$$\ln\left(\frac{\beta}{T^2}\right) = \ln\left(\frac{kR}{E}\right) + 0.6073 - \frac{E}{RT} \quad (3)$$

Due to $(\ln(kR/E) + 0.6073)$ has no relation to β/T^2, E can be calculated by the slope $(-E/R)$ of the straight line plotted by eqn (3) with $\ln(\beta/T^2)$ as the y-axis and $1/T$ as the x-axis.

2.5 Physicochemical property analysis

Viscosity of pure [BMIM]HSO_4 and [BMIM]HSO_4/ethanol with different [BMIM]HSO_4 mass concentration was measured by a Rheometer (MCR302, Anton Paar, Austria) under plate

viscosity mode. Ultimate analysis of MCEL and PCEL was analyzed by an elemental analyzer (Vario Macro Cube Elementar, Germany). FTIR spectra was scanned by a Fourier transform infrared spectrometer (ALPHA, German Brucker, German) with a wave number of 4000–400 cm^{-1} under ATR mode. Raman spectrometer (DXR-2, Thermo Fisher Scientific, U.S.) was used to character the structure of MCEL and PCEL with a wave number of 3500–100 cm^{-1}. The crystal form and crystal structure of MCEL and PCEL was established by X-ray power diffraction (XRD, Ultima IV, Rigaku UIV, Japan) using Cu radiation source ($\lambda = 0.15406$ nm) with operating voltage at 40 kV and 40 mA in scan range from 5° to 45° with a scan rate of 0.5° s^{-1} and step size 0.02°. The surface structures of MCEL and PCEL were scanned by a scanning electron microscope (SEM, VEGA, TESCAN, China) with accelerating voltage HV = 25.00 kV. Laser Particle Sizer (Jinan Winner Particle Instrument Co., LTD, China) was used to measure the particle size of MCEL and PCEL with sample concentration 10.4‰ in water, with testing range from 0.01–2000 μm.

3. Results and discussion

3.1 Viscosity characterization of [BMIM]HSO_4/ethanol

Fig. 2 illustrated the viscosity of [BMIM]HSO_4/ethanol with the [BMIM]HSO_4 mass concentration changing from 0% to 100%. Pure [BMIM]HSO_4 has a viscosity as high as 1885 mpa s, while the viscosity of [BMIM]HSO_4/ethanol reduced with the addition of ethanol as indicated in Fig. 2. As [BMIM]HSO_4 mass concentrations lower than 60%, the viscosity increased slowly with [BMIM]HSO_4 mass concentrations, and was lower than 16.68 mpa s. Low viscosity benefits the full-contact and well-interaction of cellulose with [BMIM]HSO_4, and makes it easy to recycle [BMIM]HSO_4/ethanol. The viscosity sharply increased from 16.68 mpa s to 350.29 mpa s with [BMIM]HSO_4 concentrations from 60% to 70%. The viscosity quickly increased to 1885.13 mpa s with [BMIM]HSO_4 concentrations from 70% to 100%. As [BMIM]HSO_4 mass concentrations higher than 60%, high viscosity made it difficult to stir and completely blend [BMIM]HSO_4 with cellulose. Hence, [BMIM]HSO_4/ethanol with [BMIM]HSO_4 mass concentrations 0–60% were employed to pre-treat cellulose in this study. Pure [BMIM]HSO_4 was used as control experiment to analyze the effects of co-solvent [BMIM]HSO_4/ethanol on the PCEL thermal behaviors.

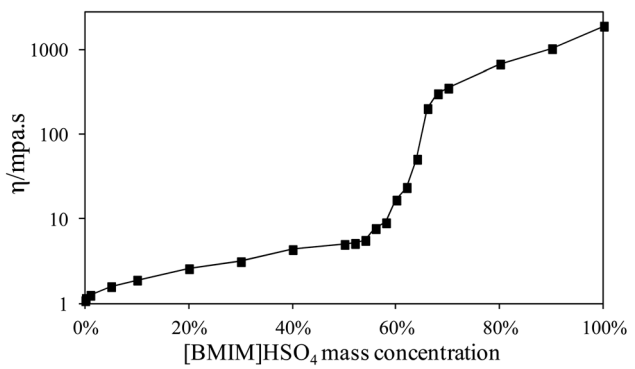

Fig. 2 Viscosity of [BMIM]HSO_4/ethanol with the [BMIM]HSO_4 mass concentration changing from 0% to 100%.

3.2 Thermal behavior of MCEL and PCEL

Thermal behaviors of MCEL and PCELs were analyzed by TG as shown in Fig. 3. Effects of four main pretreatment factors were investigated, including [BMIM]HSO_4 mass concentration (0–100%), pretreatment temperature (80–200 °C), pretreatment time (1–16 h), and the solid–liquid mass ratio ($m_{MCEL} : m_{[BMIM]HSO_4/ethanol} = 1 : 1–1 : 20$). The recovery yields of PCEL under different conditions were larger than 95%, except PCEL100% and PCEL pre-treated at 180 °C and 200 °C. Just small amount of cellulose was dissolved in [BMIM]HSO_4/ethanol, indicating that the solubility of cellulose was low in [BMIM]HSO_4/ethanol. Most of cellulose was remained as PCEL, and the recovery yields of PCEL under different conditions were provided in ESI Fig. SI1.†

Fig. 3(a) and (b) illustrated TG and DTG curves of MCEL, [BMIM]HSO_4 and PCEL0%–PCEL100%. [BMIM]HSO_4 and MCEL had one main weight loss region from 341.8 °C to 411.9 °C, and from 320.2 °C to 394.6 °C, respectively. For MCEL, the maximum weight loss rate (D_{max}, 3.10%/°C) was attained at 373.4 °C. TG and DTG curves of PCEL0% (pre-treated by ethanol) in Fig. 3(a) and (b) were similar with those of MCEL, which indicated that ethanol pretreatment had less effects on the thermal behavior of PCEL. Obvious differences were observed in TG and DTG curves of PCEL0%–PCEL60%. With [BMIM]HSO_4 mass concentration increasing from 0% to 60%, TG curves shifted to lower temperatures. Table 1 listed thermogravimetric parameters of MCEL, pure [BMIM]HSO_4 and PCEL0%–PCEL100%. The start temperature (T_i) for main weight loss of PCEL0.1%–PCEL60% shifted to a lower temperature than MCEL, even the mass concentration of [BMIM]HSO_4 was as low as 0.1%. T_i shifted from 394.3 °C for PCEL0% and 369.1 °C for PCEL60% as listed in Table 1, indicating that higher [BMIM]HSO_4 mass concentration led to a lower T_i of PCEL.

For PCEL0.1% and PCEL1%, just one weight loss peak was observed at 310–390 °C in DTG curves. Quite interestingly in Fig. 3(b), there were two weight loss peaks observed in DTG curves of PCEL5%–PCEL60%, which located in the temperature regions of 240–310 °C and 310–390 °C, respectively. The first weight loss peak at 240–310 °C was observed at [BMIM]HSO_4 concentration ≥ 5%. The maximum weight loss rate of first weight loss peak (D_{max1}) increased with [BMIM]HSO_4 mass concentration increasing to 60%. This new weight loss peak did not belong to the loss of [BMIM]HSO_4, since the weight loss temperature of [BMIM]HSO_4 was as high as 341.8–411.9 °C. [BMIM]HSO_4/ethanol pretreatment would possibly change the physical or chemical structures of cellulose. Halder *et al.*[22] found that 1-ethyl-3-methylimidazolium acetate ([Emim][OAc]) pre-treatment altered the hydrogen bonds of cellulose and produced amorphous cellulose structure in sugarcane straw. Jiang *et al.*[4] found that the physical structures of regenerated cellulose was relatively loose and disordered as amorphous cellulose, which caused the thermal stability of cellulose reducing. Amorphous cellulose was degraded more rapidly and decomposed at a lower temperature. The formation of new

Table 1 Thermogravimetric parameters of MCEL, pure [BMIM]HSO_4 and PCEL0%–PCEL100%

Name	T_i[a] (°C)	T_t[b] (°C)	T_{max1}[c] (°C)	D_{max1}[d] (% °C^{-1})	T_{max2}[c] (°C)	D_{max2}[d] (% °C^{-1})	M_r[e] (%)
MCEL	320.2	394.6	—	—	373.4	3.10	7.68
[BMIM]HSO_4	341.8	411.9	—	—	380.8	2.59	8.74
PCEL0%	320.8	394.3	—	—	377.9	2.44	10.59
PCEL0.1%	307.5	395.0	—	—	360.2	2.30	5.03
PCEL1%	273.6	394.7	—	—	352.4	1.70	6.35
PCEL5%	249.6	293.0	265.2	0.15	353.7	1.43	8.47
PCEL10%	244.4	388.1	275.1	0.43	342.4	1.28	9.35
PCEL20%	232.1	396.0	277.4	0.58	340.6	1.02	11.45
PCEL40%	321.9	369.1	277.8	0.57	340.2	1.00	13.45
PCEL60%	229.4	369.1	273.6	0.69	334.0	0.75	13.87
PCEL100%	313.3	401.4	—	—	369.5	2.13	6.31

[a] T_i is the temperature of thermal decomposition at which the main weightless zone begins. [b] T_t is the temperature of thermal decomposition at which the main weightless zone finishes. [c] T_{max1} and T_{max2} are the temperature corresponding to the first and second peak of DTG curve, respectively. [d] D_{max1} and D_{max2} are the weight loss rate corresponding to the first and second peak of DTG curve, respectively. [e] M_r is the final residue amount after thermal pyrolysis.

structures, such as amorphous cellulose and/or new intermediate structures, accounted for the first weight loss peak of PCEL.[4,22] The second weight loss peak was located at the same temperature region (310–390 °C) with MCEL. Peak temperature (T_{max2}) of the second peak shifted to a lower temperature with [BMIM]HSO_4 mass concentration increasing. The maximum weight loss rate (D_{max2}) decreased with [BMIM]HSO_4 mass concentration increasing from 0.1% to 60%. This peak would be caused by the weight loss of the remained body structure of raw MCEL.[9]

As mentioned above, the high viscosity of pure [BMIM]HSO_4 made it impossible to stir during the pretreatment process. Hence, in this study, PCEL100% was prepared by pure [BMIM]HSO_4 without stir, and was recovered by injecting ethanol after pretreatment. TG and DTG curves of PCEL100% in Fig. 3(a) and (b) slightly moved to a lower temperature region than MCEL, but at a higher temperature region than PCEL0.1%–PCEL60%. The high viscosity of [BMIM]HSO_4 prevented the full interaction of cellulose and [BMIM]HSO_4, leading to the low efficiency of pretreatment.[14,15] The addition of ethanol can efficiently reduce the viscosity of [BMIM]HSO_4 as illustrated in Fig. 2, which can break the molecular interaction of [BMIM]HSO_4. It permitted the [BMIM]HSO_4 molecular to move relatively free and easily interact with cellulose.[11] Hence, [BMIM]HSO_4/ethanol, with [BMIM]HSO_4 mass concentration lower than 60%, can efficiently pre-treat cellulose. As illustrated in Table 1, final residue yields increased with the increasing [BMIM]HSO_4 mass concentration. PCEL0.1% and PCEL1% had a lower residue yield than MCEL, while PCEL pre-treated by ≥5% [BMIM]HSO_4/ethanol had a higher residue yield than MCEL.

Effects of pretreatment temperature, pretreatment time, and solid–liquid mass ratio on the thermal behavior of PCEL were investigated based on TG and DTG curves in Fig. 3(c)–(h). Fig. 3(c) and (d) showed small changes were observed in TG and DTG curves of PCEL at different temperatures, indicating that pretreatment temperature showed weak effects on the thermal behavior of PCEL. Two different weight loss peaks were observed at 240–310 °C and 310–390 °C for PCEL20%. D_{max1} was lower than D_{max2} at each temperature. It was also noticed that the variation trend of D_{max1} and D_{max2} with pretreatment temperature were opposite. This result indicated that the structures for the first weight loss peak and the second weight loss peak were interconnected during the pretreatment process. Similar results were also observed for PCEL20% with pretreatment time ≤ 4 h (Fig. 3(e) and (f)), and for PCEL20% with $m_{MCEL} : m_{[BMIM]HSO_4/ethanol} \geq 1:5$ (Fig. 3(g) and (h)). For PCEL20% with longer pretreatment time (8 h and 16 h), or lower $m_{MCEL} : m_{[BMIM]HSO_4/ethanol}$ (1 : 1), three main weight loss peaks were observed at 240–295 °C, 295–337 °C, and 337–390 °C, respectively. The maximum rate of the three weight loss peaks (named as D_{max1}, D_{max2}, D_{max3}) reduced in the order of $D_{max3} > D_{max2} > D_{max1}$.

Above all, [BMIM]HSO_4/ethanol, instead of pure [BMIM]HSO_4, can be applied to pre-treat cellulose, and decrease the energy requirement of cellulose thermal decomposition. Compared TG and DTG curves in Fig. 3, effects of [BMIM]HSO_4 mass concentration on the thermal behavior of cellulose were the strongest among the four factors. What's more, thermal behavior of cellulose can be controlled by adjusting the [BMIM]HSO_4 mass concentration of [BMIM]HSO_4/ethanol. Hence, we focused on the physicochemical properties and thermal behaviors of PCEL0%–PCEL60% in the following study.

3.3 Physicochemical property of PCEL0%–PCEL60%

FTIR spectra and Raman spectra (Fig. SI2 in ESI†) of PCEL0%–PCEL60% were almost the same with MCEL, indicating the pretreatment of [BMIM]HSO_4/ethanol did not obviously change the chemical structures of cellulose. As listed in Table 2, no nitrogen was detected from PCEL0.1% and PCEL1%. For PCEL5%–PCEL60%, nitrogen content of PCEL increased with the [BMIM]HSO_4 mass concentration. The variation trend of nitrogen content was consistent with the variation of first weight loss peak appeared in DTG curves of PCEL5%–PCEL60% in Fig. 3(b). Nitrogen in PCEL5%–PCEL60% came from [BMIM]HSO_4, indicating that partial [BMIM]HSO_4 was remained and combined with the cellulose molecular in PCEL.

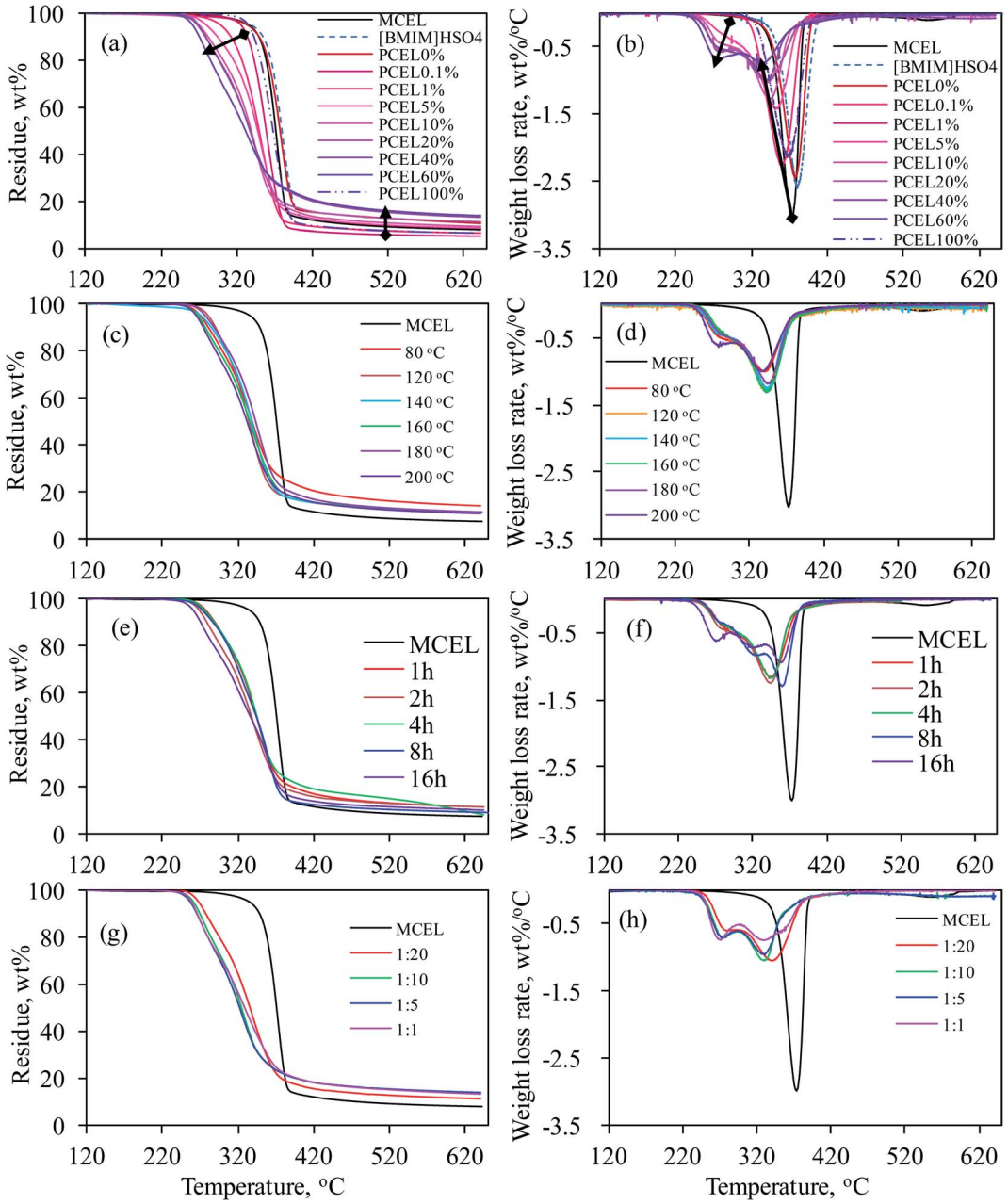

Fig. 3 TG and DTG curves of MCEL, [BMIM]HSO_4 and PCELs: (a) and (b) for [BMIM]HSO_4 mass concentration at 0–100%; (c) and (d) for pretreatment temperatures at 80–200 °C; (e) and (f) for pretreatment time for 1–16 h; (g) and (h) for solid–liquid mass ratio at 1 : 20–1 : 1.

XRD patterns of MCEL and PCEL in Fig. 4 showed that two diffraction peaks represent the typical crystal structures of cellulose, *viz.* I_α (triclinic) at $2\theta = 16°$, and cellulose I_β (monoclinic) at $2\theta = 22°$,[23] respectively. As [BMIM]HSO_4 mass concentration increased from 0% to 60%, the crystallinity index (CrI) of PCEL gradually decreased from 82.35% for MCEL to 39.62% for PCEL60%. The reduced CrI with [BMIM]HSO_4 mass concentration indicated that partial crystal structure of cellulose collapsed with the increasing [BMIM]HSO_4 mass concentration. Characterized by SEM in Fig. 5, MCEL surface was smooth, and PCEL surface was rough and cracked after pretreated at higher [BMIM]HSO_4 concentration. No obvious changes were observed on the particle size by SEM. The cumulative distribution diagram (Fig. 6) of particle size by laser particle sizer showed that particle size of MCEL was 149–174 μm with less amount of particles in the region of 0.453–4.47 μm. For PCEL, particles in the region of 0.453–4.47 μm increased slightly with the [BMIM]HSO_4 concentration increasing to 1%, and then increased largely from 8.80% to 100% with the [BMIM]HSO_4 mass concentration increasing from 5% to 60%. It was obvious that the particle size shifted to smaller values with the increasing [BMIM]HSO_4 concentration. The smaller particle size benefitted the heating transfer and promoted PCEL thermal decomposition at low temperature.[24] Hence, the T_{max} of

Table 2 Ultimate analysis of MCEL and PCEL0%–PCEL60%

Name	N [%]	C [%]	H [%]	O[a] [%]
MCEL	0.00	43.16	5.789	51.051
PCEL0%	0.00	43.16	5.789	51.051
PCEL0.10%	0.00	43.20	6.081	50.719
PCEL1%	0.00	43.24	6.084	50.676
PCEL5%	0.02	44.25	6.287	49.463
PCEL10%	0.03	44.10	6.303	49.597
PCEL20%	0.15	43.60	6.198	50.202
PCEL40%	1.62	43.96	6.200	49.840
PCEL60%	2.01	44.19	6.254	49.556

[a] Calculated by the differences.

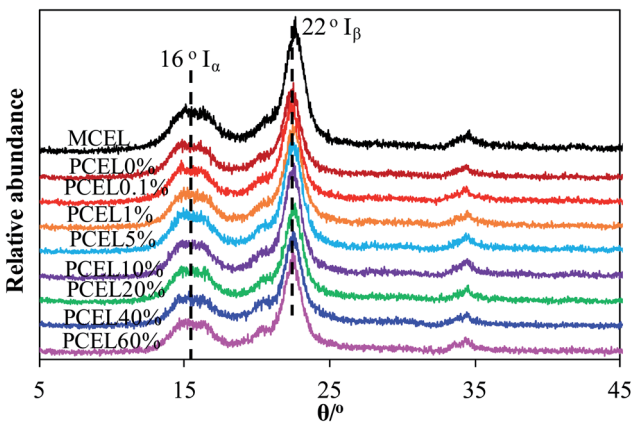

Fig. 4 XRD patterns of MCEL and PCEL0%–PCEL60%.

PCEL thermal decomposition reduced with [BMIM]HSO_4 mass concentration.

3.4 Kinetic analysis of PCEL thermal behavior

The global activation energy (E) reflected overall thermal stability of the sample. The larger the E, the higher the energy required for sample decomposition and the better the thermal stability of the sample. TG experiments of MCEL and PCEL0%–PCEL60% were conducted at 20 °C min^{-1}, 40 °C min^{-1} and 80 °C min^{-1}, which were served for the E calculation (as Fig. SI3†). E of MCEL and PCEL0%–PCEL60% were determined by DAEM. Published reports have proven that the DAEM method was quite accurate for the estimation of E.[4,23,25] In this study, α were chosen to calculate E, ranging from 0.05 to 0.95 with the step-size of 0.05. The Arrhenius plots, $\ln(\beta/T^2)$ *vs.* $1/T$, at a given α depict straight lines, which slopes can be used to calculate E. The value of correlation coefficients (R^2) was all higher than 0.9 which represented the reliability and accuracy of E. The calculated E of MCEL and PCEL0%–PCEL60% were illustrated in Fig. 7. E of MCEL was around 214–221 kJ mol^{-1}, almost stable at $\alpha = 0.1$–0.9. E is 208 kJ mol^{-1} at $\alpha = 0.05$, which was caused by the release of small and/or free molecules in samples. E increased to 268 kJ mol^{-1} at $\alpha = 0.95$, which is the final stage of cellulose pyrolysis to gradually cyclize and aromatize with a small amount of light gases.

In terms of PCEL0%, E increased gradually from 216 kJ mol^{-1} to 254 kJ mol^{-1} at $\alpha = 0.1$–0.9, which is higher than E of MCEL as shown in Fig. 7. With the addition of [BMIM]HSO_4, E variation of PCEL showed very different trends at different [BMIM]HSO_4 mass concentration. [BMIM]HSO_4/ethanol pretreatment reduced the thermal stability, and the initial stage of the thermal decomposition occurred at low temperatures. Hence, all PCEL have a lower

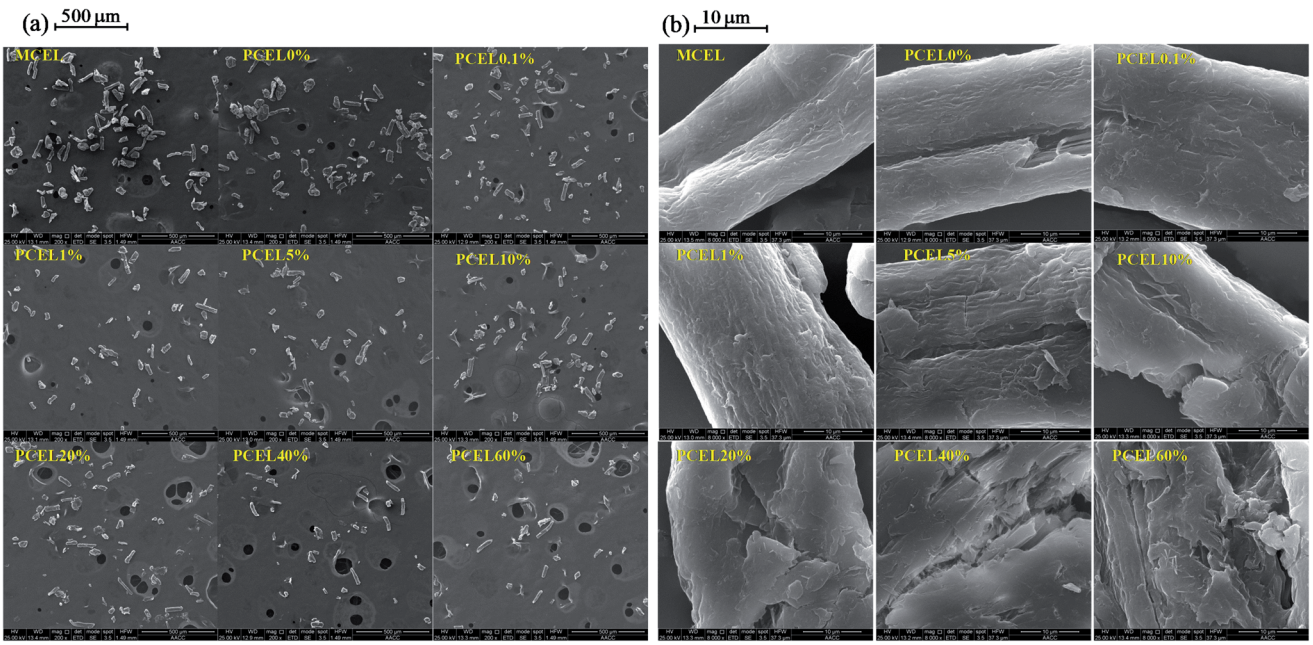

Fig. 5 SEM of MCEL and PCEL0%–PCEL60% at 140 °C: (a) 500 μm; (b) 10 μm.

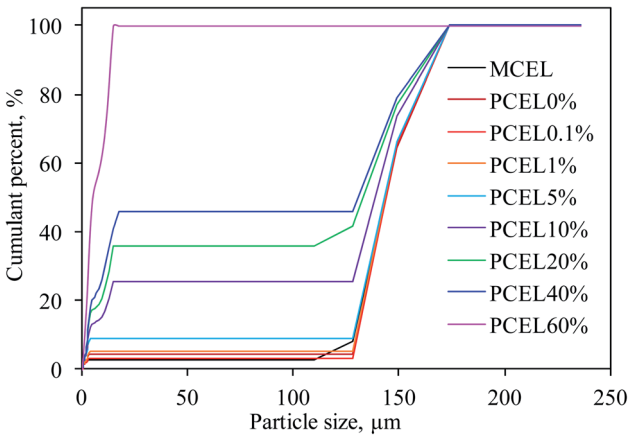

Fig. 6 The cumulative distribution of particle size of MCEL and PCEL0%–PCEL60% at 140 °C.

E than MCEL at lower α. In terms of PCEL0.1% and PCEL1%, E increased gradually from 195 kJ mol^{-1} to 224 kJ mol^{-1} and 165.0 kJ mol^{-1} to 214.4 kJ mol^{-1} at α = 0.05–0.95, respectively. With [BMIM]HSO_4 concentration increasing from 5% to 60%, three E_a stages were observed: E of PCEL in the first stage was much lower than MCEL, and increased with the α increasing from 0.05 to 0.45. This stage corresponded to the first peak of DTG curves in Fig. 3. It was well known that due to an enormous number of hydrogen bonds, MCEL was well-ordered crystalline, and has strong interactions between the molecular units, with packed and thermal-stable structure. To break the highly ordered structure is a higher barrier of the initial stage of MCEL thermal decomposition, which showed a high E at lower α. In MCEL, the structure and connection mode of each molecular unit were very similar. When the temperature raised to a certain extent, the structure concentratedly collapsed, and a large-scale decomposition reaction occurred rapidly. Hence, E stayed at a same level during MCEL thermal decomposition. Literature reported that anions of ILs acted as an H-bond acceptor,[4,14] leading to the well-ordered crystalline of cellulose broken and collapsed. The loose and disordered structure promoted the heating transfer and volatile releasing, and caused the decreased temperature of thermal decomposition with lower energy requirement. E in the second stage stayed at a stable level which is similar with E of MCEL. This stage corresponded to the second peak of DTG curves in Fig. 3, which was caused by the decomposition of original body structures. E in the final stage increased obviously at α = 0.8–0.95, which was much higher than that of MCEL.

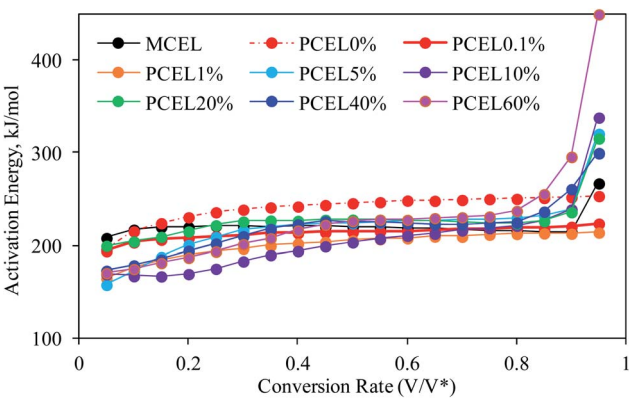

Fig. 7 The calculated E of MCEL and PCEL0%–PCEL100% at 140 °C.

3.5 Repetitive-use performance of [BMIM]HSO_4/ethanol

[BMIM]HSO_4/ethanol, without further treatment, was reused ten times to pre-treat MCEL at 140 °C with [BMIM]HSO_4 mass concentration as 1% and 20%. The [BMIM]HSO_4/ethanol was separated with PCEL by filtration, and then directly reused to pre-treat fresh MCEL. TG and DTG curves to test the repetitive-use performance of [BMIM]HSO_4/ethanol were illustrated in Fig. SI4.† For 1% [BMIM]HSO_4/ethanol, no obvious variations of TG and DTG curves indicated that [BMIM]HSO_4/ethanol had a good repetitive-use performance to pre-treat cellulose. For 20% [BMIM]HSO_4/ethanol, TG and DTG curves slightly moved to high temperatures. The possible reason was: after pretreatment, partial [BMIM]HSO_4 was remained on PCEL, causing the reduce of [BMIM]HSO_4 mass concentration.

4. Conclusion

[BMIM]HSO_4/ethanol as a binary solvent system is efficient to pre-treat cellulose, which has a low viscosity to adequately interacting with MCEL and to be easily reused. Thermal behavior and kinetic parameters of PCEL were investigated by TG and DAEM. Two or three main weight loss stages were observed for the thermal decomposition of PCEL pre-treated by [BMIM]HSO_4/ethanol, while just one weight loss peak was observed for PCEL pre-treated by ethanol and pure [BMIM]HSO_4. TG and DTG curves shifted to a lower temperature regions with the increasing [BMIM]HSO_4 mass concentration. [BMIM]HSO_4 mass concentration had strong effects on the thermal behavior of cellulose. The thermal behaviors of cellulose can be controlled by adjusting the [BMIM]HSO_4 mass concentration. In a word, co-solvents of [BMIM]HSO_4/ethanol can efficiently lower the thermal stability of PCEL, and promoting the thermal decomposition of PCEL at low temperature with a lower energy requirement. However, the interaction mechanism of [BMIM]HSO_4/ethanol pretreatment is expected to be investigated in the future work.

Conflicts of interest

There are no conflicts to declare.

Acknowledgements

This work was supported by Natural Science Foundation of Jiangsu Province (Grant No. BK20190156), the Applied Basic Research Programs of Xuzhou (Grant No. KC19048), and Science and Technology Project of Xuzhou (Grant No. KC21286).

References

1 R. Gerardy, D. P. Debecker, J. Estager, P. Luis and J. C. M. Monbaliu, *Chem. Rev.*, 2020, **120**(15), 7219–7347, DOI: 10.1021/acs.chemrev.9b00846.

2 X. Chen, S. Song, H. Li, G. Gözaydın and N. Yan, *Acc. Chem. Res.*, 2021, **54**, 1711–1722, DOI: 10.1021/acs.accounts.0c00842.

3 N. S. A. Rasid, A. Shamjuddin, A. Z. A. Rahman and N. A. S. Amin, *J. Cleaner Prod.*, 2021, **321**, 129038, DOI: 10.1016/j.jclepro.2021.129038.

4 L. Jiang, Q. Lin, Y. Lin, F. Xu, X. Zhang, Z. Zhao and H. Li, *Bioresour. Technol.*, 2020, **305**, 123044, DOI: 10.1016/j.biortech.2020.123044.

5 S. Kudo, Z. Zhou, K. Norinaga and J.-I. Hayashi, *Green Chem.*, 2011, **13**, 3306, DOI: 10.1039/C1GC15975E.

6 W. Wang and D. J. Lee, *Bioresour. Technol.*, 2021, **339**, 125587, DOI: 10.1016/j.biortech.2021.125587.

7 M. Brunner, H. Li, Z. Zhang, D. Zhang and R. Atkin, *Fuel*, 2019, **236**, 306–312, DOI: 10.1016/j.fuel.2018.09.004.

8 H. Wang, G. Gurau and R. D. Rogers, *Chem. Soc. Rev.*, 2012, **41**, 1519–1537, DOI: 10.1039/C2CS15311D.

9 A. Xu, Y. Wang, C. Li, Z. Xiao and R. Liu, *RSC Adv.*, 2019, **9**, 20976, DOI: 10.1039/C9RA03979A.

10 R. P. Swatloski, S. K. Spear, J. D. Holbrey and R. D. Rogers, *J. Am. Chem. Soc.*, 2002, **124**, 4974–4975, DOI: 10.1021/ja025790m.

11 A. Xu, L. Chen and J. Wang, *Macromolecules*, 2018, **51**, 4158–4166, DOI: 10.1021/acs.macromol.8b00724.

12 A. Salama and P. Hesemann, *ACS Sustainable Chem. Eng.*, 2020, **49**, 17893–17907, DOI: 10.1021/acssuschemeng.0c06913.

13 A. Xu and F. Wang, *Green Chem.*, 2020, **22**, 7622–7664, DOI: 10.1039/D0GC02840A.

14 B. Nis and B. K. Ozsel, *Renewable Energy*, 2021, **169**, 1051–1057, DOI: 10.1016/j.renene.2021.01.083.

15 A. Xu, Y. Zhang, Y. Zhao and J. Wang, *Carbohydr. Polym.*, 2013, **92**, 540–544, DOI: 10.1016/j.carbpol.2012.09.028.

16 A. Xu, L. Cao and B. Wang, *Carbohydr. Polym.*, 2015, **125**, 249–254, DOI: 10.1016/j.carbpol.2015.02.045.

17 X. Li, H. Li, Z. Ling, D. Xu, T. You, Y.-Y. Wu and F. Xu, *Macromolecules*, 2020, **53**, 3284–3295, DOI: 10.1021/acs.macromol.0c00592.

18 J. Tao, T. Kishimoto, S. Suzuki, M. Hamada and N. Nakajima, *Holzforschung*, 2016, **70**, 519–525, DOI: 10.1515/hf-2015-0116.

19 D. Kasprzak, E. Krystkowiak, I. Stepniak and M. Galinski, *Eur. Polym. J.*, 2019, **113**, 89–97, DOI: 10.1016/j.eurpolymj.2019.01.053.

20 M. Gericke, T. Liebert, O. A. El Seoud and T. Heinze, *Macromol. Mater. Eng.*, 2011, **296**, 483–493, DOI: 10.1002/mame.201000330.

21 Y. Zhang and A. Kendall, *BioEnergy Res.*, 2017, **10**, 183–198, DOI: 10.1007/s12155-016-9776-5.

22 P. Halder, S. Kundu, S. Patel, R. arthasarathy, B. Pramanik, J. Paz-Ferreiro and K. Shah, *Energy Convers. Manage.*, 2019, **200**, 112067, DOI: 10.1016/j.enconman.2019.112067.

23 X. Cao, J. Zhang, K. Cen, F. Chen, D. Chen and Y. Li, *Biomass Bioenergy*, 2021, **148**, 106061, DOI: 10.1016/j.biombioe.2021.106061.

24 X. Huang, K. Yamasaki, S. Kudo, J. Sperry and J.-I. Hayashi, *J. Anal. Appl. Pyrolysis*, 2020, **145**, 104728, DOI: 10.1016/j.jaap.2019.104728.

25 Y. Qiao, B. Wang, Y. Ji, F. Xu, P. Zong, J. Zhang and Y. Tian, *Bioresour. Technol.*, 2019, **278**, 287–295, DOI: 10.1016/j.biortech.2019.01.102.